Theoretical Study on Reaction Mechanism of the Ketenylidene Radical with Nitrogen Dioxide

Jia-xu Zhang, Jing-yao Liu, Ze-sheng Li,* and Chia-chung Sun

Institute of Theoretical Chemistry, State Key Laboratory of Theoretical and Computational Chemistry, Jilin University, Changchun 130023, People's Republic of China

Received: February 24, 2005; In Final Form: May 18, 2005

The complex doublet potential-energy surface for the reaction of CCO with NO_2, including 8 minimum isomers and 17 transition states, is explored theoretically using the coupled cluster and density functional theory. The association of CCO with NO_2 was found to be a barrierless process forming an energy-rich adduct **a** ($OCCNO_2$) followed by oxygen shift to give **b** (O_2CCNO). Our results show that the product $\mathbf{P_1}$ (CO_2 + CNO) is the major product with absolute yield, while the product $\mathbf{P_4}$ (2CO + NO) is the minor product with less abundance. The other products may be undetectable. The product $\mathbf{P_1}$ (CO_2 + CNO) can be obtained through $\mathbf{R \rightarrow a \rightarrow b \rightarrow P_1}$ (CO_2 + CNO), whereas the product $\mathbf{P_4}$ (2CO + NO) can be obtained through two channels $\mathbf{R \rightarrow a \rightarrow b \rightarrow c \rightarrow (d, g) \rightarrow P_2}$ (OCNO + CO) $\rightarrow \mathbf{P_4}$ (2CO + NO) and $\mathbf{R \rightarrow a \rightarrow b \rightarrow f \rightarrow P_3}$ (c-OCC−O + NO) $\rightarrow \mathbf{P_4}$ (2CO + NO). Because the intermediates and transition states involved in the above three channels are all lower than the reactants in energy, the CCO + NO_2 reaction is expected to be rapid, which is consistent with the experimental measurement in quality. The present study may be helpful for further experimental investigation of the title reaction.

1. Introduction

Ketenylidene, CCO, is known to be an important intermediate in a variety of chemical processes, such as hydrocarbon combustion,[1−3] molecular cloud formation in interstellar space,[4,5] and the photolysis and reactions of carbon suboxide, C_3O_2.[6,7] This radical has been the subject of several spectroscopic investigations.[8−13] However, only a few reports of kinetic measurements of CCO reactions have appeared.[14,15] On the other hand, it is known that nitrogen oxides (NO_x $x = 1, 2$) are among the major atmospheric pollutants released by combustion process. To minimize the harmful effects before their release in the atmosphere, one effective way is to chemically reduce them by the reburning of combustion products.[16−21] Reliable information on the kinetics of these reactions is of importance for modeling the combustion processes. To our best knowledge, only one experimental study has been performed on the rate constant of the CCO reaction with NO_2.[22] The measured rate constant of the CCO + NO_2 reaction at room temperature was $(6.89 \pm 0.5) \times 10^{-11}$ cm^3 $molecule^{-1}$ s^{-1}, which indicates that the CCO reaction with NO_2 is very fast and may play an important role in the fate of NO_2 pollutants during combustion processes. However, there is a lack of information on product channels, product identification, and product distributions, although this information may be important in the NO_2-involved sequential chain processes. In view of the potential importance and the rather limited experimental information, a thorough theoretical study of this reaction is therefore desirable. The main objectives of the present article are to (1) provide the elaborated isomerization and dissociation channels on the $OCCNO_2$ PES, (2) investigate the possible products of the title reaction to assist in further experiment identification, and (3) give a deep insight into the mechanism of ketenylidene−NO_2 combustion reaction.

* To whom correspondence should be addressed. Fax: +86-431-8498026. E-mail address: Zeshengli@mail.jlu.edu.cn.

2. Computational Methods

All calculations are carried out using the GAUSSIAN98 program.[23] All structures of the stationary points including reactants, minimum isomers, transition states, and products are calculated using hybrid density functional B3LYP method (the Becke's three parameter hybrid functional with the nonlocal correlation functional of Lee−Yang−Parr) with 6-311G(d,p) basis set. The stationary nature of structures is confirmed by harmonic vibrational frequency calculations, i.e., equilibrium species possess all real frequencies, whereas transition states possess one and only one imaginary frequency. The zero-point energy (ZPE) corrections are obtained at the same level of theory. To conform the transition states connecting the designated intermediates, intrinsic reaction coordinate (IRC) calculation is carried out at the B3LYP/6-311G(d,p) level. Furthermore, to make the found structure, especially for some involved in the major channel more stringent, the modified Perdew−Wang one-parameter model for kinetics (MPW1K)[24] method optimizations are performed with 6-311G(d,p) basis set. To obtain more reliable energetic data, higher-level single-point energy calculations are performed at the CCSD(T) level of theory (coupled-cluster approach with single and double substitutions including a perturbative estimate of connected triple substitutions) with the same basis set (CCSD(T)/6-311G(d,p)) by using the B3LYP/6-311G(d,p) optimized geometries. Unless otherwise specified, the CCSD(T) single-point energies with inclusion of B3LYP zero-point energies (ZPE) (simplified as CCSD(T)//B3LYP) are used in the following discussions. Meanwhile, for the purpose of comparison, we employed G2(B3LYP/MP2/CC)[25] (a modification of the Gaussian-2 approach using density functional theory) to calculate the single-point energy based on the B3LYP/6-311G(d,p) geometries. The total G2(B3LYP/MP2/CC) energy with zero-point energy (ZPE) correction is calculated as follows[25]

10.1021/jp050949d CCC: $30.25
Published on Web 07/06/2005

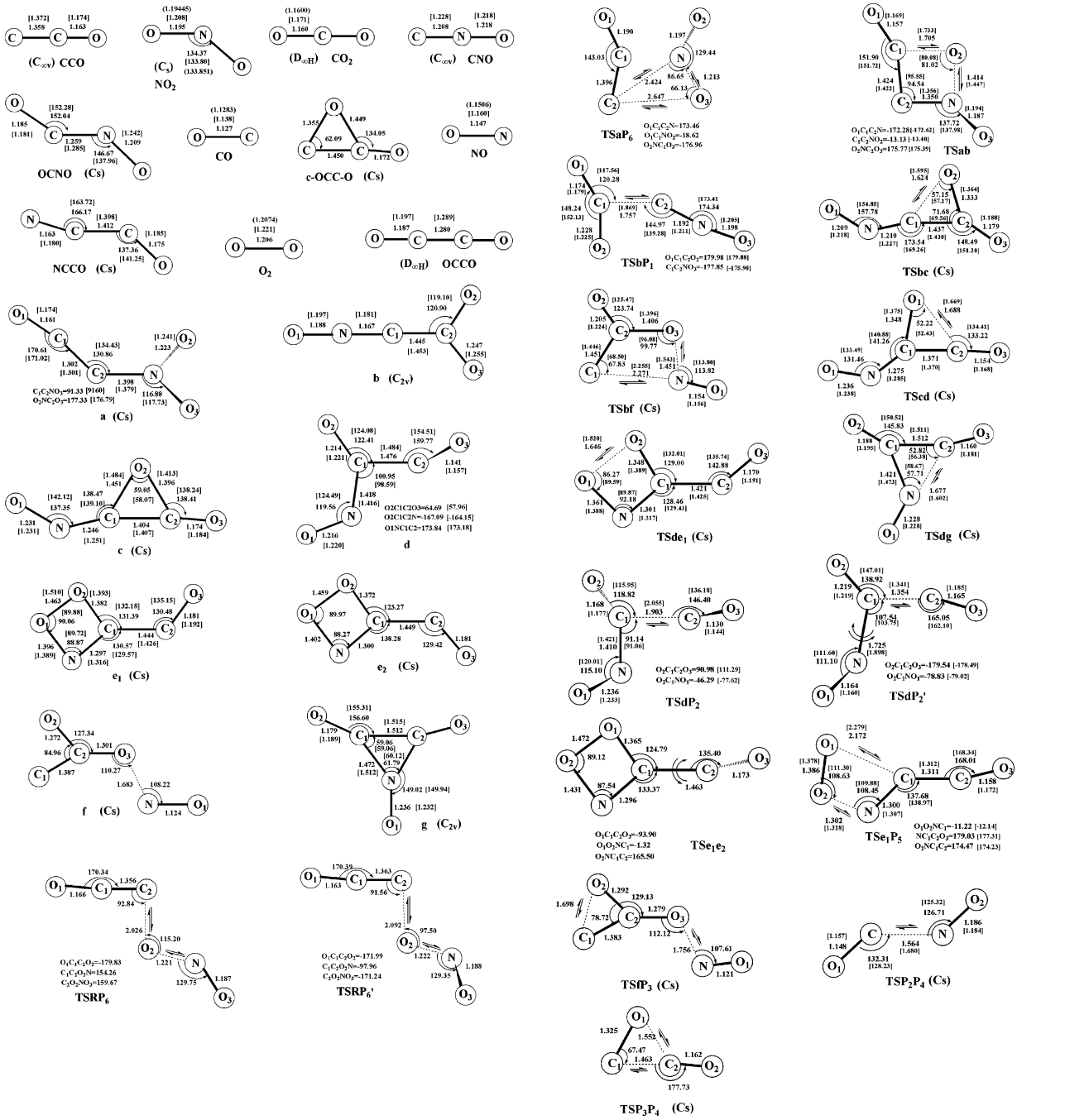

Figure 1. The B3LYP/6-311G(d,p)-optimized geometries of reactants, products, isomers, and transition states. Bond distances are in angstroms, and angles are in degrees. The values in brackets are at the MPW1K/6-311G(d,p) level and values in parentheses are the experimental values (ref 26 for NO_2, ref 27 for NO, CO, CO_2, and O_2).

$$\mathrm{E[G2(B3LYP/MP2/CC)]} = \mathrm{E[CCSD(T)/6\text{-}311G(d,p)]} + \mathrm{E[MP2/6\text{-}311{+}G(3df,2p)]} - \mathrm{E[MP2/\,6\text{-}311G(d,p)]} + \mathrm{HLC} + \mathrm{ZPE[B3LYP/6\text{-}311G(d,p)]} \times 0.98$$

where $\mathrm{HLC} = -0.00451n_\beta - 0.00019n_\alpha$ and n_α and n_β are used to denote the numbers of α and β valence electrons, respectively.

3. Results and Discussion

For the CCO + NO_2 reaction, eight intermediate isomers (denoted by the letters from **a** to **g**) including three open-chain species, four cyclic species, and one weakly bound complex are located at the B3LYP/6-311G(d,p) level. To make clear the interrelation between various isomers and products, 17 transition states (**TS**) are obtained. The optimized structures of the reactants, products, isomers, and transition states as well as the corresponding experimental values[26,27] are depicted in Figure 1 as well as the vibrational mode of the imaginary frequencies of the transition states. The geometric parameters for some species obtained by the MPW1K method are also given in this figure for comparison. The electronic states, harmonic vibrational frequencies, as well as available experimental values[27] are given in Table 1. As listed in Table 1, the theoretical and experimental results agree very well, with the largest discrepancy of 7% at the B3LYP/6-311G(d,p) level. It is known that the B3LYP method has been found to systematically underestimate barrier heights;[28] thus, in the present study the energies are improved at the highly correlated CCSD(T) level. For convenient disussions, the energy of reactants **R** is set to be zero for reference. The relative energies including ZPE corrections are

TABLE 1: Electronic States and Harmonic Vibrational Frequencies (cm^{-1}) of the Stationary Points at the B3LYP/6-311G(d,p) Level

species	state	frequencies	expt[a]
CCO	$^3\Sigma$	379, 381, 1104, 2035	379, −1063, 1967
NO_2	2A	767, 1399, 1707	750, 1318, 1618
CNO	$^2\Pi$	321, 417, 1202, 1934	
CO_2	$^1\Sigma_g$	667, 667, 1375, 2436	667,1333, 2349
OCNO	2A	266, 346, 535, 969, 1433, 2174	
CO	1A	2220	2170
c-OCC−O	1A	425, 513, 518, 942, 1263, 2053	
NO	2P	1988	1904
NCCO	^{2}A	221, 277, 566, 813, 1968, 2222	
O_2	$^3\Sigma_g^-$	1641	1580
OCCO	^{3}A	277, 311, 311, 950, 1791, 2398	
a	^{2}A	57, 144, 381, 494, 532, 616, 745, 858, 1328, 1442, 1531, 2160	
b	$^2B_2$	63, 81, 407, 407, 524, 536, 698, 699, 1095, 1360, 1527, 2413	
c	^{2}A	142, 164, 356, 405, 538, 622, 665, 831, 1075, 1365, 1810, 2106	
d		120, 156, 237, 346, 460, 504, 602, 789, 900, 1499, 1628, 2134	
$\mathbf{e}_1$	^{2}A	164, 179, 362, 526, 658, 695, 843, 860, 1085, 1277, 1624, 1922	
$\mathbf{e}_2$	^{2}A	178, 196, 249, 491, 665, 706, 847, 872, 1117, 1313, 1579, 1925	
f	^{2}A	91, 121, 142, 242, 367, 538, 567, 718, 980, 1351, 1636, 1995	
g	$^2B_1$	127, 158, 251, 393, 409, 626, 676, 901, 921, 1338, 1830, 1886	
TSab		431i, 153, 367, 589, 611, 644, 675, 935, 1008, 1125, 1722, 2093	
TSbc	^{2}A	430i, 121, 166, 355, 417, 557, 633, 785, 1123, 1366, 1954, 2144	
TSbf	^{2}A	253i, 147, 241, 305, 517, 605, 628, 645, 946, 1235, 1707, 1859	
$\mathbf{TSbP}_1$		444i, 51, 127, 362, 447, 470, 584, 682, 1210, 1320, 2067, 2110	
TScd	^{2}A	384i, 171, 194, 360, 414, 593, 602, 872, 1185, 1376, 1708, 2196	
$\mathbf{TSde}_1$	^{2}A	961i, 161, 208, 371, 484, 601, 655, 858, 1088, 1295, 1563, 1986	
TSdg	^{2}A	149i, 143, 264, 268, 399, 521, 615, 859, 992, 1355, 1780, 1984	
$\mathbf{TSdP}_2$		289i, 82, 120, 237, 248, 361, 402, 631, 740, 1393, 1887, 2160	
$\mathbf{TSdP}_2$		174i, 113, 219, 230, 315, 327, 639, 673, 910, 1639, 1759, 2139	
$\mathbf{TSe}_1\mathbf{e}_2$		223i, 161, 291, 444, 583, 684, 825, 857, 1080, 1275, 1549, 1980	
$\mathbf{TSe}_1\mathbf{P}_5$		826i, 140, 160, 447, 496, 590, 733, 765, 940, 1062, 1616, 2195	
$\mathbf{TSfP}_3$	^{2}A	305i, 62, 117, 161, 377, 501, 557, 680, 982, 1267, 1606, 1980	
$\mathbf{TSRP}_6$		510i, 52, 109, 150, 202, 462, 542, 700, 1091, 1156, 1643, 2036	
$\mathbf{TSRP}_6$		483i, 57, 134, 176, 208, 459, 536, 708, 1083, 1184, 1653, 2034	
$\mathbf{TSP}_2\mathbf{P}_4$	^{2}A	575i, 166, 359, 593, 1657, 2032	
$\mathbf{TSP}_3\mathbf{P}_4$	1A	376i, 469, 475, 912, 1336, 2084	

[a] Experimental values from ref 27.

TABLE 2: Relative Energies (RE) (kcal mol^{-1}) (with Inclusion of the B3LYP/6-311G(d,p) ZPE Corrections) for the Stationary Points at the B3LYP/6-311G(d,p), CCSD(T)/6-311G(d,p)//B3LYP/6-311G(d,p), and G2(B3LYP/MP2/CC)//B3LYP/6-311G(d,p) Levels

species	B3LYP	CCSD(T)//B3LYP	G2//B3LYP	species	B3LYP	CCSD(T)//B3LYP	G2//B3LYP
R $^3CCO + NO_2$	0.0	0.0	0.0	$\mathbf{TSaP}_6$	12.8	14.2	6.5
$\mathbf{P}_1$ CO_2 + CNO	−96.4	−99.3	−103.0	TSbc	−69.4	−63.5	−73.4
$\mathbf{P}_2$ OCNO + CO	−101.6	−105.3	−107.5	TSbf	0.8	−3.3	−11.5
$\mathbf{P}_3$ c-OCC−O + NO	−32.8	−44.7	−48.7	$\mathbf{TSbP}_1$	−76.2	−70.1	−77.9
$\mathbf{P}_4$ CO + CO + NO	−118.2	−141.1	−137.4	TScd	−67.7	−62.3	−71.9
$\mathbf{P}_5$ NCCO + $^3O_2$	−46.3	−49.8	−38.1	$\mathbf{TSde}_1$	−16.7	−16.6	−24.7
$\mathbf{P}_6$ ^{3}OCCO + NO	−77.0	−74.2	−73.5	TSdg	−79.0	−76.7	−83.8
a	−45.7	−39.2	−49.3	$\mathbf{TSdP}_2$	−73.4	−70.8	−86.7
b	−79.5	−72.5	−80.8	$\mathbf{TSdP}_2$	−81.3	−81.8	−78.0
c	−70.5	−66.1	−75.4	$\mathbf{TSe}_1\mathbf{e}_2$	−14.3	−17.9	−28.4
d	−84.1	−80.2	−87.5	$\mathbf{TSe}_1\mathbf{P}_5$	−2.9	7.4	−3.5
$\mathbf{e}_1$	−20.4	−24.1	−34.2	$\mathbf{TSfP}_3$	−7.0	−8.8	−16.3
$\mathbf{e}_2$	−19.1	−23.2	−33.2	$\mathbf{TSRP}_6$	13.5	17.0	12.8
f	−6.5	−9.6	−17.2	$\mathbf{TSRP}_6$	13.3	16.4	12.1
g	−79.5	−77.4	−84.7	$\mathbf{TSP}_2\mathbf{P}_4$	−95.4	−104.4	−105.0
TSab	−24.8	−20.7	−33.5	$\mathbf{TSP}_3\mathbf{P}_4$	−33.2	−45.2	−48.8

listed in Table 2. By means of the transition states and their connected isomers or products, a schematic potential-energy surface (PES) of the CCO + NO_2 reaction in doublet is plotted in Figure 2. Moreover, to further testify the reaction mechanism obtained at the CCSD(T)//B3LYP level, we performed additional G2(B3LYP/MP2/CC) single-point energy calculations for all stationary points. The comparison between the calculated results of two higher levels is made. In addition, the potential curves of the initial N-attack of the CCO radical to NO_2 are presented in Figure 3.

a. Initial Association. The attack of the terminal C atom of triplet CCO at NO_2 molecule may have three possible ways, i.e., middle-N attack, end-O attack, and side-NO π-bonding attack. The middle-N attack can form the chainlike C_s-symmetried isomer **a** ($OCCNO_2$). It should be noted that the attempt to locate the transition state from **R** to **a** at the B3LYP/6-311G(d,p) level failed. To further confirm this process with or without a barrier, we calculate the pointwise potential curve at the B3LYP/ 6-311G(d,p) level (in Figure 3). The calculations are performed by pointwise optimization, which means that optimization for the other geometric parameters is done with every fixed internal C−N bond length. It is obvious that this addition process is a barrierless association. We noticed that further optimization of the minimum with C−N distance of 1.4 Å, as presented in Figure 3, leads to **a** at the B3LYP/6-311G-(d,p) level. Figure 3 shows that the adduct **a** is formed as the end C atom of CCO and middle N atom of NO_2 approach each other to interact on an attractive potential energy surface. The binding energy of **a**, which is −39.2 kcal/ mol at the CCSD-(T)//B3LYP level of theory, indicates this process makes the adduct (**a**) highly activated so that further isomerization or dissociation reactions can be promoted. The association is

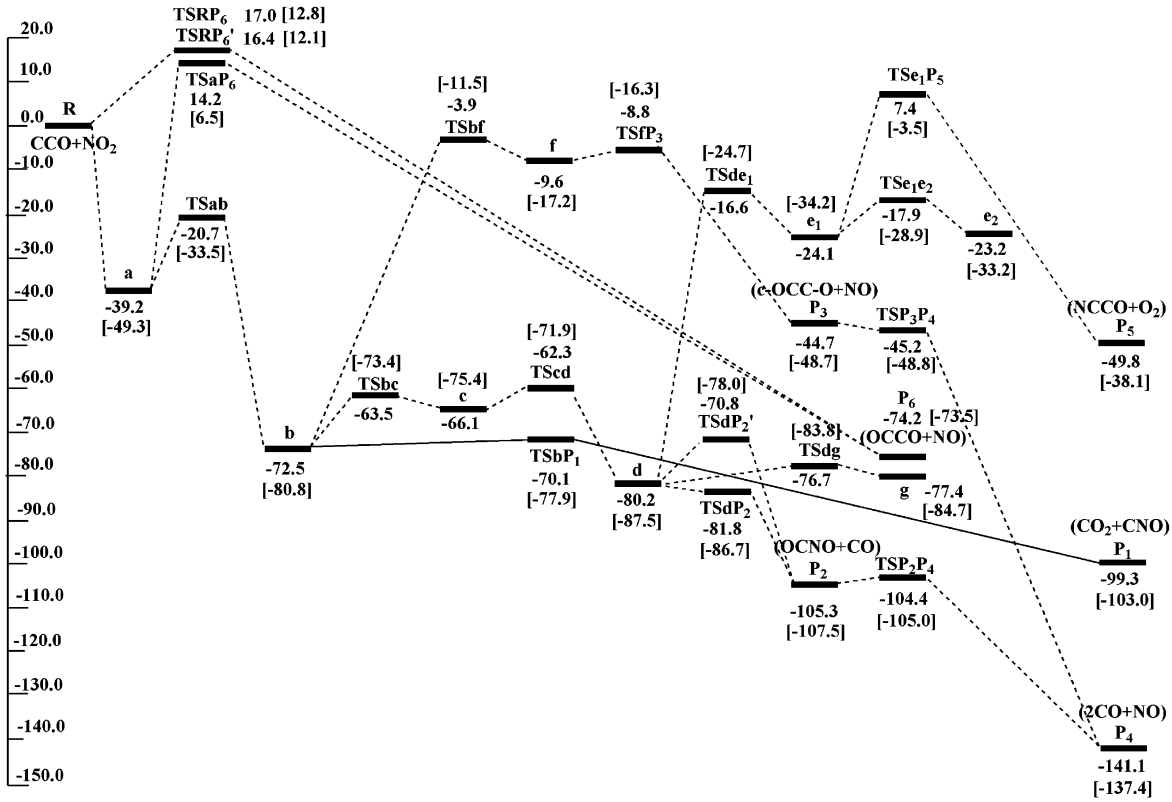

Figure 2. Schematic potential energy surface of the reaction channels for the CCO + NO_2 reaction at the CCSD(T)/6-311G(d,p)//B3LYP/6-311G-(d,p) + ZPE level. The values in brackets are obtained at the G2(B3LYP/MP2/CC)//B3LYP/6-311G(d,p) level. E_{rel} are the relative energies (kcal mol^{-1}).

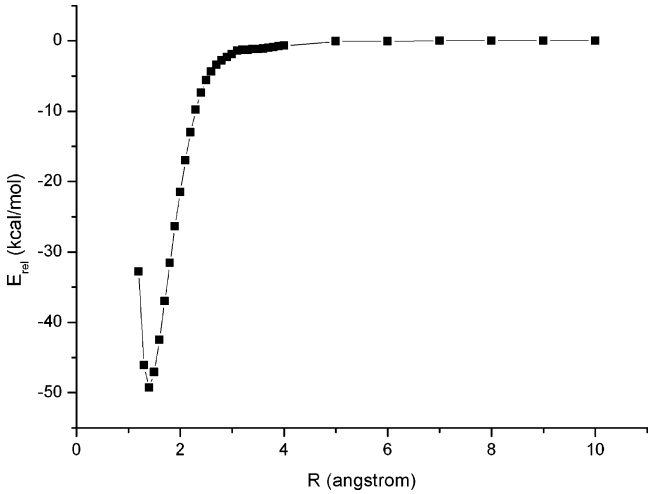

Figure 3. Relaxed potential-energy curve for the formative process of the adduct (**a**) at the B3LYP/6-311G(d,p) level. *R* is the value of C−N distance. E_{rel} are the relative energies (kcal mol^{-1}).

expected to be fast and to play a significant role in the reaction kinetics. The end-O attack can directly lead to product $\mathbf{P_6}$ (OCCO + NO) via the transition state $\mathbf{TSRP_6}$ or $\mathbf{TSRP_{6'}}$, which lies 17.0 or 16.4 kcal/mol above **R**. Then, the end-O attack is a considerably barrier-consumed process. The C_1-symmetried $\mathbf{TSRP_6}$ and $\mathbf{TSRP_{6'}}$ may be distinguished according to attack tendency. The calculations predict 2.2 and 2.3% stretching of the breaking N−O bond, as compared to the N−O equilibrium bond length of NO_2, and 70.7 and 67.8% stretching of the forming C−O bond with respect to the C−O length of OCCO in $\mathbf{TSRP_6}$ and $\mathbf{TSRP_{6'}}$, respectively. Thus, $\mathbf{TSRP_6}$ and $\mathbf{TSRP_{6'}}$ are reactantlike and this reaction process proceeds via an "early" transition state. Optimization of the side-NO π bonding attacking isomer usually leads to the middle-N attack species **a** or the end-O attack product $\mathbf{P_6}$ (OCCO + NO). For the attacking pathway of the middle-C atom or O atom of the triplet CCO, despite numerous attempts, we cannot succeed in locating any transition states or isomers. Thus, we can find from Figure 2 that only the terminal-C of CCO attacking at the middle-N of NO_2 to form adduct **a** is the most favorable association channel for the title reaction. For simplicity, in the following discussions, we mainly discuss the formation pathways of various products starting from **a**.

b. Isomerization and Dissociation Pathways. The initially formed middle-N attack isomer **a** ($OCCNO_2$) with C_s symmetry can isomerize to the branched species **b** (O_2CCNO) with C_{2v} symmetry via a 1,3-O shift from N to C_1 atom (i.e., **TSab**). The barrier of this process is 18.5 kcal/mol. The transition state **TSab** has a nonplanar four-membered ring structure with C_1 symmetry. The migrating oxygen is 1.414 Å away from the origin and 1.705 Å away from the migrating terminus. Isomer **b** then can easily lead to product $\mathbf{P_1}$ (CO_2 + CNO) via $\mathbf{TSbP_1}$. Only 2.4 kcal/mol barrier is needed to overcome for this process. $\mathbf{TSbP_1}$ with C_1 symmetry is characterized by a slightly elongated C−C bond (1.757 Å at the B3LYP/6-311G(d,p) level). The vibrational mode of imaginary frequency of $\mathbf{TSbP_1}$ corresponds to the C−C bond stretch vibration. Such a multistep process can be described as

Path $\mathbf{P_1}$: $\mathbf{R \rightarrow a \rightarrow b \rightarrow P_1}$ (CO_2 + CNO). The isomer **b** (O_2CCNO) can alternatively proceed via a ring-closure transition state (**TSbc**) to form the CCO three-membered ring isomer **c** (c-C(O)OC−NO) followed by ring opening via **TScd** to give the lowest-lying isomer **d** (OCC(O)NO). **d** can readily interconvert to each other with the second lowest lying species **g**

(c-C(O)C(O)N−O), which has a tight CCN three-membered ring structure via transition state **TSdg**. This process involves a small barrier not more than 3.5 kcal/mol. As seen in Figure 1, All **TSbc**, **TScd**, and **TSdg** may be viewed as tight three-membered ring species with C_s symmetry of respective $^2A'$, $^2A'$, and $^2A''$ electronic states. The distances of C_1-O_2 in **TSbc**, C_2-O_2 in **TScd**, and C_2-N in **TSdg** are 1.624, 1.688, and 1.677 Å, respectively. The imaginary frequency of respective 430i, 384i, and 149i mainly involve C_1-O_2, C_2-O_2, and C_2-N bond stretch vibrations. In addition, the conversion barriers of **b** → **c**, **c** → **d**, and **d** → **g** are rather low, 9, 3.8, and 3.5 kcal/mol, respectively, which indicates the easy interconversion between each other. Subsequently, **d** can directly dissociate to product **P2** (OCNO + CO) through the direct C−C bond cleavage via the transition states **TSdP2** or **TSdP2′**. These processes can simply be written as

Path P2: R → a → b → c → (d, g) → P2 (OCNO + CO). **TSdP2** is a C_1-symmetried branched-chain structure. The decomposing C−C bond (1.903 Å) indicates the formation of two products OCNO and CO. Note that the relative energy of **TSdP2** is 1.6 kcal/mol lower than **d** at the CCSD(T)/6-311G-(d,p)//B3LYP/6-311G(d,p) level, which indicates that intermediate **d** is kinetically very unstable toward dissociation. Interestingly, we locate one alternative transition state **TSdP2′** connecting **d** and **P2** tested by IRC calculations, which lies higher than **TSdP2** by about 11 kcal/mol. **TSdP2′** has also branched-chain structure with C_1 symmetry. The distance of C−N is surprisingly long as 1.724 Å, while the C−C bond that will be broken is surpringly short as 1.354 Å. The dissociation process from **d** to **P2** via **TSdP2′** is one of the O-atom rotations around the C−N bond along with C−N bond elongation and C−C bond contraction. Subsequently, the C−N bond continuously rotates with its shortening and C−C bond lengthens, till rupture. Because a higher potential barrier is involved in this process, the reaction pathway via **TSdP2** to form **P2** is much more favorable.

In addition, **b** can also undergo NO migration from the C_1 atom to the O_3 atom via transition-state **TSbf** to form the C_s-symmetried weak-bound complex **f** (C(O)CONO) with a relatively long O−N bond (1.683 Å). The loose CCNO four-membered ring on plan is found in **TSbf**, which has C_s symmetry and $^2A''$ electronic state. Because the **b** → **f** conversion barrier is rather high, 68.6 kcal/mol, it is not easy to form **f**. In addition, **f** easily dissociates to **P3** (c-OCC−O + NO) with a very small barrier of only 0.8 kcal/mol. The **f** → **P3** conversion is the single O_3-N bond rupture along with C_1 and O_2 atoms ring-closure process through transition-state **TSfP3**. The branched-chain **TSfP3** is C_s symmetrized with the $^2A''$state. The imaginary frequency of 305i mainly involves C_1-O_2 and $N-O_3$ bonds breath vibration. The formation pathway of **P3** is

Path P3: R → a → b → f → P3 (c-OCC−O + NO). The isomer **a** can isomerize to form product **P6** (OCCO + NO) through a simple 1,2 O shift associated with a cleavage of the C_2-N single bond via **TSaP6**. As shown in Figure 1, **TSaP6** presents an abnormally loose three-membered ring structure. The distances of C_2-N and C_2-O_3 are surprisingly long as 2.424 and 2.647 Å, respectively, while the $N-O_3$ bond that will be broken is surprisingly short as 1.213 Å. Morover, the C_1-N distance is relatively short as 1.757 Å. This makes **TSaP6** more like the attack of the middle-C atom in CCO at the N atom in NO_2 to form adduct species ($O(C)CNO_2$). However, the IRC calculations confirm the connection of **TSaP6** between **a** and **P6**. Since the dissociation transition-state **TSaP6** lies 14.2 kcal/mol above reactants **R**, this process is kinetically unfeasible for the title reaction. The O_1 and O_2 ring closure of **d** via **TSde1** leads to a four-membered ring species **e1** (c-OONC−CO), intermediates **e1** and **e2** are cis and trans isomers in terms of O_3 atom. The interconversion between them takes place via a C−C single rotation transition state **TSe1e2**. The process involves a low internal rotation barrier (6.2 kcal/mol above **e1**) because of the long C−C single-bond length (**e1** 1.444 Å, **e2** 1.449 Å). The dissociation from **e1** to **P5** (NCCO + O_2) needs to overcome a barrier about 31.5 kcal/mol, and **TSe1P5** is 7.4 kcal/mol higher than **R**, thus, the product **P5** is surely energetically inaccessible. All **TSde1**, **TSe1e2**, and **TSe1P5** have the OONC four-membered ring forms. **TSde1** has C_s symmetry with $^2A'$ electronic state, while both **TSe1e2** and **TSe1P5** are C_1 symmetrized.

Finally, let us discuss the secondary dissociation reaction of the primary products **P2** (OCNO + CO) and **P3** (c-OCC−O + NO). As we can see in Figure 2, there is only 0.9 kcal/mol barrier height for C−N bond rupture in **P2**, and **TSP3P4** is even 0.5 kcal/mol below **P3** at the CCSD(T)/6-311G(d,p)//B3LYP/6-311G(d,p) level, which means that the cricoid species c-OCC−O is unstable and will likely decompose to 2CO. Consequently, further direct dissociation of OCNO in **P2** and c-OCC−O in **P3** to form the same secondary product **P4** (2CO + NO) may be very facile due to the lower dissociation barriers. **TSP2P4** has C_s-symmetry chain structure with a $^2A''$ state, while **TSP3P4** has CCO three-membered ring structure with C_s symmetry and $^1A'$ electronic state.

Since there is lack of available experimental parameters for the isomers and transition states involved in the reaction, for comparison, we performed optimization calculations for some species present on the feasible pathways at another commonly used level of theory, i.e., MPW1K method with 6-311G(d,p) basis set. Several studies[24,29,30] have demonstrated that the MPW1K model gives remarkably good performance for kinetics and geometries. As is shown in Figure 1, our calculated geometries agree well with experimental results with the largest deviation of 0.3% at B3LYP/6-311G(d,p) level and 0.9% at MPW1K/6-311G(d,p) level. The structure parameters at both levels are in reasonable agreement with each other. The large deviation in bond distance lies in the O−O bonding of **TSde1** (0.126 Å) and C−N bonding of **TSP2P4** (0.116 Å). The large bond angle deviation lies in **TSdP2** (10.22°) and **TSdP2′** (8.09°). It should be pointed out that, in **Path P3**, isomer **f** (C(O)CONO), product c-OCC−O, and transition states **TSfP3** and **TSP3P4** cannot be obtained using the MPW1K method. IRC calculations show that isomer **b** can directly dissociate to c-OCC−O and NO through C−N bond rupture along with ring closure of C_1 and O_2 atoms via **TSbf**. While at the MPW1K/6-311G(d,p) level, optimization of c-OCC−O species always leads to separate fragments 2CO. Therefore, in despite of the complicated conversion processes, we consider that **b** will directly lead to the final product **P4** (2CO + NO) after clearing the high barrier of **TSbf** at MPW1K/6-311G(d,p) level. In addition, optimization of isomer **e2** (c-OONC−CO) usually leads to isomer **d** (OCC-(O)NO), and the internal rotation transition state **TSe1e2** cannot be located also at MPW1K/6-311G(d,p) level. However, such discrepancies lie in unfavorable pathways and will not affect our discussions on the reaction mechanism.

c. Reaction Mechanism. On the basis of the reaction pathways obtained in the last sections, let us discuss the mechanism of the CCO + NO_2 reaction. Here, for easier discussion, the most possible reaction pathways of three primary products **P1** (CO2 + CNO), **P2** (OCNO + CO), **P3** (cOCC−O + NO), and one secondary product **P4** (2CO + NO) are listed again:

Path P_1: **R→ a → b → P_1** (CO_2 + CNO);

Path P_2: **R → a → b → c → (d, g) → P_2** (OCNO + CO) → **P_4** (2CO + NO);

Path P_3: **R → a → b → f → P_3** (c-OCC−O + NO) → **P_4** (2CO + NO).

The CCO radical can barrierlessly react with NO_2 at the middle-N site to form adduct **a** ($OCCNO_2$) followed by isomerization to **b** (O_2CCNO), which was involved in all reaction pathways. Starting from **b**, **Path P_3** to form product **P_3** is relatively negligible due to the rather large barrier (69.2 kcal/mol) from **b** to **f**. With respect to the other pathways, the transition state **TSbP_1** (−70.1 kcal/mol) in **Path P_1** lies lower than **TSbc** (−63.5 kcal/mol) and **TScd** (−62.3 kcal/mol) in **Path P_2**; moreover, compared to **Path P_2**, pathway **Path P_1** is a relatively simple dissociation process, in which only considerably small dissociation barrier of 2.4 kcal/mol is needed to overcome. In view of these factors, **Path P_1** is much more feasible than **Path P_2**. When secondary dissociation procedure is considered, most of the products **P_2** and **P_3** may lead to **P_4**. As reflected in the final product distributions, product **P_1** may dominate, while **P_4** may occupy only a small part. **P_2** and **P_3** are too much less abundant to be detectable.

It is useful to make comparison for the mechanism of the title reaction between the CCSD(T)//B3LYP and G2(B3LYP/MP2/CC)//B3LYP results. It is readily found that the features of PESs obtained at both levels are generally in parallel. (1) **Path P_1** may be the most feasible pathway; (2) **Path P_2** may be the second feasible pathway which has less competition with **Path P_1**; (3) **Path P_3** should be the least favorable pathway. However, as can be seen from Table 2, the G2(B3LYP/MP2/CC)//B3LYP energies are lower than CCSD(T)//B3LYP energies in general. Thus, at the G2(B3LYP/MP2/CC)//B3LYP level, the pathway of **e_1** (c-OONC−CO) dissociation to **P_5** (NCCO + O_2) via **TSe_1P_5** become kinetically feasible. However, this pathway cannot compete with **Path P_1**, **Path P_2**, and **Path P_3** and is still of very minor importance. Thus, it is seen that in quality the reaction mechanism as well as the possible products is very similar at the two higher levels; we expect that the present CCSD(T)//B3LYP results could be reliable for the title reaction.

4. Conclusions

A detailed doublet potential energy surface of the CCO + NO_2 reaction system has been characterized at the B3LYP and CCSD(T) (single-point) levels of theory. The mechanism can generally be summarized as association, isomerization, and dissociation processes.

a. Initially, the terminal-C atom of CCO radical can barrierlessly attack the N atom of NO_2 to form isomer **a** ($OCCNO_2$), which converts to the low-lying C_{2v}-symmetried species **b** (O_2-CCNO). Yet, the terminal-C attack of CCO radical at the end-O of NO_2 has to overcome a barrier at least 16.4 kcal/mol leading to **P_6** (OCCO + NO), indicative of its negligible contribution at normal temperatures.

b. Isomer **b** can directly dissociate to product **P_1** (CO_2 + CNO) as the most feasible primary dissociation product. Alternatively, **b** can undergo successive isomerization and fission processes to **P_2** (OCNO + CO) and **P_3** (c-OCC−O + NO), both of which can further decompose to **P_4** (2CO + NO) as the less competitive product. Because only the total rate constant is experimentally available, the present theoretical studies may provide useful information on the reaction mechanism and assist in further laboratory identification of the products.

Acknowledgment. This work is supported by the National Natural Science Foundation of China (20333050, 20303007), the Doctor Foundation by the Ministry of Education, the Foundation for University Key Teacher by the Ministry of Education, the Key Subject of Science and Technology by the Ministry of Education of China, and the Key Subject of Science and Technology by Jilin Province.

References and Notes

(1) Bayes, K. D. *J. Chem. Phys.* **1970**, *52*, 1903.
(2) Becker, K. H.; Bayes, K. D. *J. Chem. Phys.* **1968**, *48*, 653.
(3) Fontijn, A.; Johnson, S. E. *J. Chem. Phys.* **1973**, *59*, 6193.
(4) Ohishi, M.; Suzuki, H.; Ishikawa, S.; Yamada, C.; Kanamori, H.; Irvine, W. M.; Brown, R. D.; Godfrey, P. D.; Kaifu, N. *Astrophys.* **1991**, *380*, 39.
(5) Brown, R. D.; Cragg, D. M.; Godfrey, P. D.; Irvine, W. M.; McGonagle, D. *J. Intl. Soc. Study Origin Life* **1992**, *21*, 399.
(6) Willis, C.; Bayes, K. D. *J. Am. Chem. Soc.* **1967**, *88*, 3202.
(7) Strayss, C. E. M.; Kable, S. H.; Chawla, G. K.; Houston, P. L.; Burak, I. R. *J. Chem. Phys.* **1990**, *94*, 1837.
(8) Yamada, C.; Kanamori, H.; Horiguchi, H.; Tsuchiya, S.; Hirota, E. *J. Chem. Phys.* **1986**, *84*, 2573.
(9) Moazzen-Ahmadi, N.; Boere, R. T. *J. Chem. Phys.* **1999**, *110*, 955.
(10) Moazzen-Ahmadi, N.; Boere, R. T. *J. Chem. Phys.* **1998**, *108*, 6588.
(11) Ohashi, N.; Kiryu, R.; Okino, S.; Fujitake, M. *J. Mol. Spectrosc.* **1993**, *157*, 50.
(12) Fujitake, M.; Kiryu, R.; Ohashi, N. *J. Mol. Spectrosc.* **1992**, *154*, 169.
(13) Becker, K. H.; Horie, O.; Schmidt, V. H.; Wiesen, P. *Chem. Phys. Lett.* **1982**, *90*, 64.
(14) Bauer, W.; Becker, K. H.; Meuser, R. *Ber. Bunsen−Ges. Phys. Chem.* **1985**, *89*, 340.
(15) Donnelly, V. M.; Pitts, W. M.; McDonald, J. R. *Chem. Phys.* **1980**, *49*, 289.
(16) Baren, R. E.; Erickson, M. A.; Hershberger, J. F. *Int. J. Chem. Kinet.* **2002**, *34*, 12.
(17) Rim, K. T.; Hershberger, J. F. *J. Phys. Chem. A* **1998**, *102*, 4592.
(18) (a) Lanier, W. S.; Mulholland, J. A.; Beard, J. T. *Symp. (Int.) Combust., [Proc.]* **1988**, *21*, 1171. (b) Chen, S. L.; McCarthy, J. M.; Clark, W. D.; Heap, M. P.; Seeker, W. R.; Pershing, D. W. *Symp. (Int.) Combust., [Proc.]* **1988**, *21*, 1159.
(19) Myerson, A. L. In *15th Symposium (International) on Combustion*; The Combustion Institute: Pittsburgh, PA, 1975; p 1085.
(20) Song, Y. H.; Blair, D. W.; Siminski, V. J.; Bartok, W. In *18th Symposium (International) on Combustion*; The Combustion Institute: Pittsburgh, PA, 1981; p 53.
(21) Chen, S. L.; McCarthy, J. M.; Clark, W. D.; Heap, M. P.; Seeker, W. R.; Pershing, D. W. In *21st Symposium (International) on Combustion*; The Combustion Institute: Pittsburgh, PA, 1986; p 1159.
(22) Thweatt, W. D.; Erickson, M. A.; Hershberger, J. F. *J. Phys. Chem. A* **2004**, *108*, 74.
(23) Frisch, M. J.; Trucks, G. W.; Schlegel, H. B.; Scuseria, G. E.; Robb, M. A.; Cheeseman, J. R.; Zakrzewski, V. G.; Montgomery, J. A.; Stratmann, R. E.; Burant, J. C.; Dapprich, S.; Millam, J. M.; Daniels, A. D.; Kudin, K. N.; Strain, M. C.; Farkas, O.; Tomasi, J.; Barone, V.; Cossi, M.; Cammi, R.; Mennucci, B.; Pomelli, C.; Adamo, C.; Clifford, S.; Ochterski, J.; Petersson, G. A.; Ayala, P. Y.; Cui, Q.; Morokuma, K.; Malick, D. K.; Rabuck, A. D.; Raghavachari, K.; Foresman, J. B.; Cioslowski, J.; Oritz, J. Gomperts, R.; Martin, R. L.; Fox, D. J.; Keith, T.; Al-Lanham, M. A.; Peng, Johnson, B. G.; Chen, W.; Wong, M. W.; Andres, J. L.; Head-Gordon, M.; Replogle, E. S.; Pople, J. A. *Gaussian 98*, revision A.9; Gaussian, Inc.; Pittsburgh, PA, 1998.
(24) Lynch, B. J.; Fast, P. L.; Harris, M.; Truhlar, D. G. *J. Phys. Chem. A* **2000**, *104*, 4811.
(25) Bauschlicher, C. W.; Partridge, H. *J. Chem. Phys.* **1995**, *103*, 1788.
(26) Kuchitsu, K. *Structure of Free Polyatomic Molecules Basic Data*, 1998.
(27) Lide, D. R. In *CRC Handbook of Chemistry and Physics*, 80th ed.; CRC Press: Boca Raton, 1999.
(28) Lynch, J.; Fast, P. L.; Harris, M.; Truhlar, D. G. *J. Phys. Chem. A* **2002**, *104*, 4811.
(29) Lynch, B. J.; Truhlar, D. G. *J. Phys. Chem. A* **2001**, *105*, 2936.
(30) Lynch, B. J.; Truhlar, D. G. *J. Phys. Chem. A* **2002**, *106*, 842.